Biosensors and Bioelectronics 136 (2019) 97–105

Contents lists available at ScienceDirect

Biosensors and Bioelectronics

journal homepage: www.elsevier.com/locate/bios

Sensitive and specific detection of *E. coli* using biomimetic receptors in combination with a modified heat-transfer method

Peter Cornelis[a,*], Stella Givanoudi[a,b], Derick Yongabi[a], Heiko Iken[c], Sam Duwé[d], Olivier Deschaume[a], Johan Robbens[b], Peter Dedecker[d], Carmen Bartic[a], Michael Wübbenhorst[a], Michael J. Schöning[c], Marc Heyndrickx[b,e], Patrick Wagner[a,**]

[a] KU Leuven, Department of Physics and Astronomy, Laboratory for Soft Matter and Biophysics, Celestijnenlaan 200 D, B-3001, Leuven, Belgium
[b] Flanders Research Institute for Agriculture, Fisheries and Food, ILVO, Animal Sciences Unit & Technology and Food Unit, Burgemeester Van Gansberghelaan 92, B-9820, Merelbeke, Belgium
[c] Institute of Nano- and Biotechnologies, Aachen University of Applied Sciences, Heinrich-Mußmann-Straße 1, 52428, Jülich, Germany
[d] KU Leuven, Department of Chemistry, Laboratory for Nanobiology, Celestijnenlaan 200 G, B-3001, Leuven, Belgium
[e] Ghent University, Department of Pathology, Bacteriology and Avian Diseases, Salisburylaan 133, B-9820, Merelbeke, Belgium

ARTICLE INFO

Keywords:
Heat transfer
Biomimetic sensors
E. coli
Surface-imprinted polymers

ABSTRACT

We report on a novel biomimetic sensor that allows sensitive and specific detection of *Escherichia coli* (*E. coli*) bacteria in a broad concentration range from 10^2 up to 10^6 CFU/mL in both buffer fluids and relevant food samples (i.e. apple juice). The receptors are surface-imprinted polyurethane layers deposited on stainless-steel chips. Regarding the transducer principle, the sensor measures the increase in thermal resistance between the chip and the liquid due to the presence of bacteria captured on the receptor surface. The low noise level that enables the low detection limit originates from a planar meander element that serves as both a heater and a temperature sensor. Furthermore, the experiments show that the presence of bacteria in a liquid enhances the thermal conductivity of the liquid itself. Reference tests with a set of other representative species of *Enterobacteriaceae*, closely related to *E. coli*, indicate a very low cross-sensitivity with a sensor response at or below the noise level.

1. Introduction

Recently, biosensors have been developed for food safety and quality evaluation in food, feed, and environmental applications because of their advantageous rapidity and ease of use (Mehrotra, 2016). Crucial for a proficient (bio)sensor is the development of recognition elements with high affinity and specificity (Chambers et al., 2008; Morales and Halpern, 2018; Van Dorst et al., 2010). Specifically for microbes, be it pathogenic or other bacteria in the environment or food, the limitations associated with certain classical biorecognition elements and/or with a workable transducing system have led to a situation in which sensors are tested in lab conditions only, while not being suitable for real life samples. In this work, we show that synthetic polymer receptors combined with the heat transfer method (HTM) close this gap.

Surface-imprinted polymers (SIPs) are a type of biomimetic receptor that is already established as being selective in detecting its target (Eersels et al., 2013; Hayden et al., 2006). They can be synthesized in various ways (Eersels et al., 2016), and can also be coupled to a wide variety of detection platforms such as: Quartz-crystal microbalance (QCM) (Dickert et al., 2001; Yilmaz et al., 2015), surface plasmon resonance (SPR) (Perçin et al., 2017; Yilmaz et al., 2015), electro-chemical impedance spectroscopy (EIS) (Golabi et al., 2017), and thermal wave transport analysis (TWTA) (Steen Redeker et al., 2017). Even without a transducer platform they have applications, such as in the separation of bacteria (Schirhagl et al., 2012) and cell sorting (Ren et al., 2013).

In recent years, experiments based on the heat-transfer method (HTM) have established that small changes at the solid-liquid interface alter the efficiency of heat transfer from a solid chip to the supernatant liquid, for instance upon DNA denaturation (van Grinsven et al., 2012), binding of cells to SIPs (Eersels et al., 2013), or phase transitions in lipids (Losada-Pérez et al., 2014). Regarding cell detection, it is also known from molecular-dynamics simulations that the thermal conductivity of lipid bilayers is around four times lower than that of water

* Corresponding author. KU Leuven, Laboratory for Soft Matter and Biophysics, Celestijnenlaan 200 D, B-3001, Leuven, Belgium.
** Corresponding author. KU Leuven, Laboratory for Soft Matter and Biophysics, Celestijnenlaan 200 D, B-3001, Leuven, Belgium.
E-mail addresses: peter.cornelis@kuleuven.be (P. Cornelis), patrickhermann.wagner@kuleuven.be (P. Wagner).

https://doi.org/10.1016/j.bios.2019.04.026
Received 8 March 2019; Received in revised form 3 April 2019; Accepted 14 April 2019
Available online 24 April 2019
0956-5663/ © 2019 Elsevier B.V. All rights reserved.

Table 1
European Commission Regulation (EC) 1441/2007 of 05/12/2007 on microbiological criteria for foodstuffs and Council Directive 98/83/EC of 03/11/1998 on the quality of water intended for human consumption, and Proposal for a Directive of the European Parliament and of the Council concerning the quality of bathing water COM (2002) 581 final (EC, 2003).

Food, water, drinks	Legal limit[a] (*E. coli*)
Meat preparations	500–5000 CFU[b]/g
Cheeses (from heat treated milk)	100–1000 CFU[b]/g
Precut fruit and vegetables (ready-to-eat)	100–1000 CFU[b]/g
Unpasteurized fruit and vegetable juices (ready-to-drink)	100–1000 CFU[b]/g
Minced meat and mechanically separated meat	50–500 CFU[b]/g
Butter/Cream from raw milk or milk with lower heat treatment than pasteurization	10–100 CFU[b]/g
Live bivalve molluscs and live echinoderms, tunicates and gastropods	230 MPN[c]/100 g
Shelled and shucked products of cooked crustaceans and molluscan shellfish	1 - 10 MPN[c]/g
Water (bathing)	250–500 CFU[b]/100 mL
Water (drinking)	0 CFU[b]/100 mL

[a] The lowest value is the target value, while the highest value is the tolerance value as specified in the EC regulation 1441/2007.
[b] CFU: Colony forming units.
[c] MPN: Most probable number.

(Nakano et al., 2010). Furthermore, HTM allows to study microbial growth, for example the proliferation of *Saccharomyces cerevisiae* strains (Betlem et al., 2018). In a nutshell, HTM monitors the thermal resistivity of a sample by measuring the temperature of a heat source at the backside of the sensor chip (T_1), the temperature inside the liquid (T_2) and the power (P) required by the system to keep T_1 at a predefined value. The thermal resistance (R_{th}) is calculated by dividing the temperature difference $T_1 - T_2$ by the input power (Eq. (1)) (Lenz et al., 2000). R_{th} has the unit K/W, however we will use °C/W because only temperature differences play a role.

$$R_{th} = \frac{(T_1 - T_2)}{P} \quad (1)$$

E. coli is a relevant indicator for pathogenic enteric bacteria and for fecal contamination in environmental, food and agricultural samples, and therefore it is included in food safety regulations (see Table 1). In addition, *E. coli* is the organism of choice for the surveillance of drinking-water quality (WHO, 2011). It is also frequently used as indicator organism in research on antimicrobial resistance, biosafety, and disinfection (Dewaele et al., 2011; Persoons et al., 2010). Current detection methods for bacteria include polymerase chain reaction (PCR), bacteriological colony counting, and immunological methods. Due to their sensitivity, selectivity and reliability, PCR and colony counting are the most used for *E. coli* enumeration in food and feed, for which standardized ISO methods are available (ISO, 2001). The immunological methods employ antibody–antigen interactions to detect bacteria. The most proficient ELISA assay makes use of antibody specificity (Lazcka et al., 2007) and has a limit of detection (LoD) of 500 CFU/mL (Zhang et al., 2015). However, these methods are time-consuming and take from several hours up to days (Lazcka et al., 2007), thus hampering their use in acute situations, in which instant action is necessary. Moreover, they require trained staff and well-equipped laboratories. A recent potentiometric technique based on bacterial recognition by aptamers requires complex sample pre-treatment to remove all charged species (Zelada-Guillen et al., 2010). Currently, the detection limit for *E. coli* using HTM combined with SIPs (van Grinsven et al., 2016) or thermal wave transport analysis (TWTA) (Steen Redeker et al., 2017) is $1{\cdot}10^4$ CFU/mL, which is comparable to fluorescence microscopy (Cohen et al., 2010) and electrochemical impedance spectroscopy (EIS) (Golabi et al., 2017), meaning the LoD is too high for real life samples. The goal of this work is to significantly lower the LoD to levels that comply with the legal limits for *E. coli* in various food products and water for different purposes, as required by the European Commission regulations (Table 1).

The original implementation of the HTM (Eersels et al., 2013) has a high noise level which prohibits reaching detection limits low enough for relevant concentrations in food: The noise level on the R_{th} signal (see Eq. (1)) is the added uncertainty of the three independent parameters T_1, T_2, and P. To improve this, we replace the heating unit by a planar meander-type metallic structure that acts simultaneously as a heat source and a temperature sensor for T_1, while T_2 is measured with a calibrated Pt100 resistor at a fixed distance from the chip surface. Based on insights from our previous work (Stilman et al., 2017), the sensing device described in the present work is also designed to minimize parasitic heat losses, to improve focusing of the thermal current through the bio-sensitive chip area, and to avoid air-bubble formation.

2. Materials and methods

2.1. Materials

Squared metallic substrates of size $10 \times 10\,mm^2$ were cut from a 0.2 mm thick stainless-steel sheet (AISI 304, Finetubes web reference) and from a 0.5 mm thick aluminum sheet (Brico N.V., Leuven, Belgium). Microscope cover glasses of size $10 \times 10\,mm^2$, 0.12 mm thick were purchased from VWR international BVBA (Leuven, Belgium). The Sylgard 184 silicone elastomer kit was purchased from Malvom N.V. (Schelle, Belgium). Acetone, isopropanol, sodium dodecylsulfate (SDS), anhydrous tetrahydrofuran (THF), bisphenol A, phloroglucinol and 4,4′-diisocyanatodiphenylmethane were purchased from Sigma-Aldrich (Diegem, Belgium). Tissue culture grade Lysogeny broth and ampicillin sodium salt (91.0–102.0%) were purchased from VWR international BVBA (Leuven, Belgium). Phosphate buffer saline (PBS) solution with pH 7.4 was prepared using NaCl, Na_2HPO_4, and KH_2PO_4 purchased from Sigma-Aldrich (Diegem, Belgium). Non-cleared apple juice, meeting the requirements of the EU biolabel, was purchased from Colruyt (Heverlee, Belgium) and used as received. *Citrobacter freundii* (LMG 3246^T), *Hafnia alvei* (LMG 10392^T), *Serratia marcescens* subsp. *Marcescens* (LMG 2792^T) and *Escherichia blattae* (LMG 3030^T) cultures were provided by ILVO. The *Escherichia coli* (JM109 (DE3)) culture, a fluorescently green labeled lab-strain, was provided by the Laboratory for Nanobiology at KU Leuven. mEmerald-Paxillin-22 was a gift from M. Davidson (Addgene plasmid # 54219). The Mix & Go! *E. coli* transformation kit and buffer set was purchased from Zymo Research (Leiden, The Netherlands).

2.2. Meander-based heat source

To create the thermal gradient, which underlies the HTM principle, a meander structure was designed that is supplied with a variable current depending on the power required by the system (see Fig. 1A). The meander consists of a gold layer deposited on a 1 mm thick glass substrate ($10 \times 15\,mm^2$), using a 10 nm thick chromium adhesion layer (Bäcker et al., 2011). The gold layer is 100 nm thick and the meander lines are 100 µm wide with an interline distance of 50 µm (total length 15 cm, resistance ≈ 450 Ω). During calibration, to enable temperature measurements with the meander, the thermal coefficient of resistance (TCR) was determined as $0.0028 \pm 2{\cdot}10^{-5}\,\Omega/°C$, which is comparable to the literature value of 0.0034 Ω/°C (Resistor Guide web reference). The four contact pads allow for a highly accurate three-point delta resistance measurement of the meander, which will be discussed in detail in paragraph 2.4.

2.3. Optimized HTM device

Fig. 1B–D shows the device and its components from different perspectives. Heat losses from the heat source to the environment are

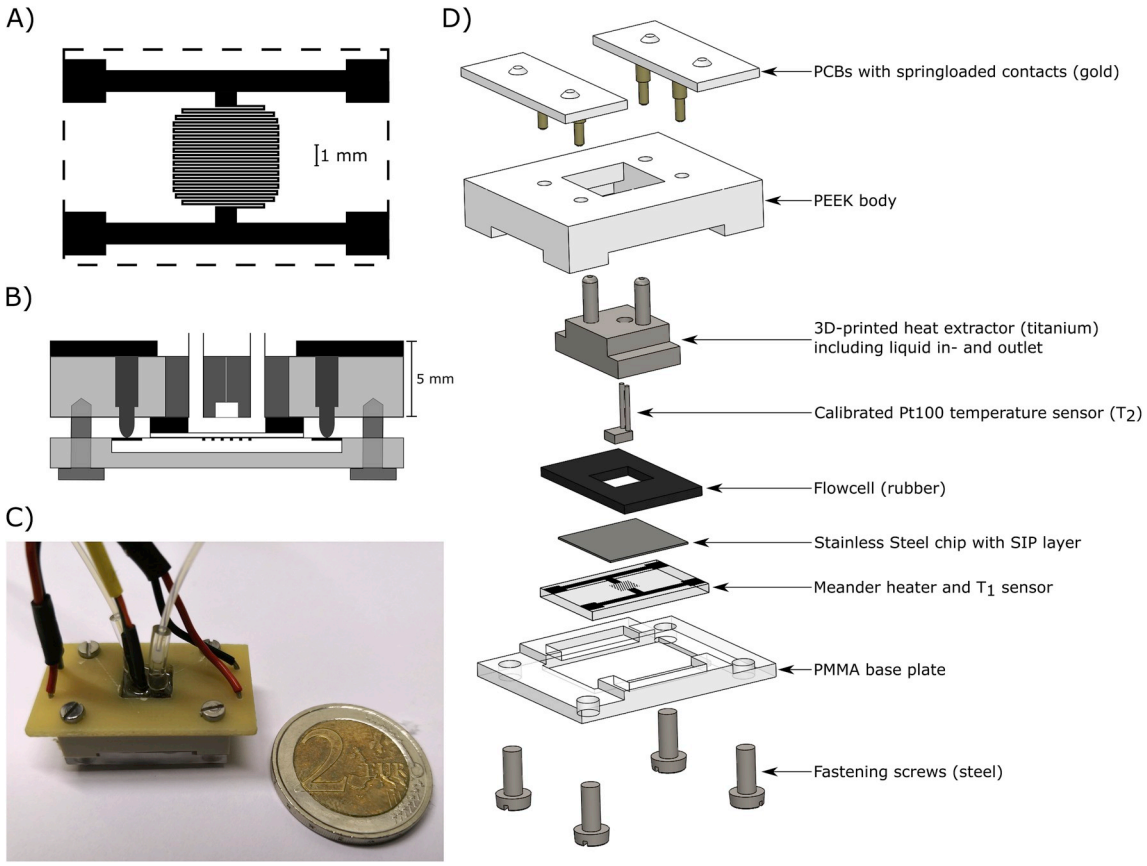

Fig. 1. A) Schematic drawing of the meander structure of the heat source also used as T_1 thermometer. The dashed line shows the dimensions of the supporting glass substrate. B) Schematic drawing of a cross-section of the HTM setup. C) Photo of the HTM-sensor device with a 2 € coin as a size reference. D) Schematic exploded view of the optimized HTM setup. All elements of the schematic drawings are drawn to scale (PEEK: Polyether ether ketone).

limited by covering its backside with poly (methyl methacrylate) (PMMA) (λ = 0.2 W/m.K). A Titanium (λ = 19.4 W/m.K) top cover on the flow cell was used to assist in directing the heat flow through the sensor chip by efficiently removing heat. A Pt100 sensor encased in this titanium top provides the second required temperature for HTM measurements. Also, the aspect ratio of the flow cell is low to achieve homogeneous heat flow and a laminar temperature profile, as suggested by Stilman et al. (2017). The flow cell compartment is 1 mm high with a surface area of 5 × 5 mm^2, resulting in an internal volume of 25 µL. Hence, the distance, over which the bacteria need to diffuse to be captured by the chip, is limited, which allows for a swift sensor response.

2.4. Electronics and software

To control the heat source, a combination of a Keithley 6221 current source and a Keithley 2182A nanovoltmeter was used. With this combination, the three-point delta measurement method is performed, which involves generating a square current wave and averaging three consecutive voltage measurements of the nanovoltmeter. Each voltage measurement was alternately taken at the center of a maximum and a minimum of the square wave. This method compensates for thermoelectric voltages and allows for accurate resistance measurements while also enabling control of the current amplitude and heating power. The Pt100 temperature sensor resistance was measured using the 4-wire resistance function of an HP 34401A digital multimeter. The entire measurement setup, including a proportional-integral-derivative controller for the heat source and remotely controlled syringe pumps (NE-500, ProSense, Oosterhout, The Netherlands), was controlled using an in-house LabView program.

2.5. Cell cultures

Bacterial species were cultured in 200 mL lysogeny broth (LB) under a 5% CO_2 atmosphere at 37.0 °C (*C. freundii*), 30.0 °C (*H. alvei*), or 28.0 °C (*E. blattae* and *S. marcescens*) for a period of 24–48 h. Additionally, fluorescently labeled *E. coli* were generated by transforming Mix & Go! competent JM109 (DE3) *E. coli* with pRSETb-mEmerald; Mix & Go! competent cells were prepared using the Zymo Research Transformation Kit, according to manufacturer's instructions. pRSETb-mEmerald was cloned by inserting the mEmerald coding sequence from mEmerald-Paxillin-22 between the *Bam*HI and *Eco*RI restriction sites of pRSETb. Transformed *E. coli* were grown for 16 h at 37.0 °C on LB agar plates supplemented with 100 µg/mL ampicillin. Liquid cultures were prepared by inoculating single colonies in 200 mL LB supplemented with 100 µg/mL ampicillin and growing the cultures for 24 h at 37.0 °C in a shaking incubator (180–210 rpm). The cells were collected by centrifugation at 7500 rpm (7239 g) for 5 min at 4.0 °C and the pellet was resuspended in 5 mL of 1 × PBS. This washing step was repeated three times to remove all LB residues from the bacterial suspension. The cell concentration of these suspensions was then determined by measuring the optical density at 600 nm (OD600) using the Ocean Optics™ Red Tide VIS-NIR Fiber Optic Spectrometer.

2.6. Synthesis of SIP receptor chips and contact angle measurements

The soft-lithographic process of depositing a polymer coating with *E. coli* imprints on stainless-steel chips was performed under inert nitrogen atmosphere. First, 122 mg of 4,4′-diisocyanatodiphenylmethane and 222 mg of bisphenol A, which are functional monomers, were dissolved in 500 mL of anhydrous tetrahydrofuran (THF) together with

25 mg of phloroglucinol cross-linker. This mixture was stirred at 65.0 °C for 200 min until the solution turned into a gel. Then, it was diluted in a 1:5 ratio in THF and spin coated for 60 s at 2000 rpm onto stainless-steel substrates. Next, a cell-covered stamp (see below) was brought into the nitrogen atmosphere and gently pressed onto the polyurethane (PU) layer. This was left to cure for 18 h at 65.0 °C. After curing and returning to normal atmosphere, the stamp was removed from the surface and bound bacteria were removed by rinsing the layer with 1% SDS and 1 × PBS, leaving behind selective binding cavities on the polymer surface (Eersels et al., 2013). Finally, the backside of the substrate was covered with 40 µm thick Scotch™ tape to provide electrical insulation against the heating- and temperature-sensing gold meander.

The polydimethylsiloxane (PDMS) stamps, used for the imprinting step, were covered with template cells by applying 400 µL of an $8{\cdot}10^8$ CFU/mL *E. coli* stock solution onto the stamp, and after 30 min sedimentation time, removing the excess liquid by spinning at 3000 rpm for 60 s. This creates a dense monolayer of template cells on the surface. The PDMS stamps (3 mm thick, 10 × 10 mm^2) were made beforehand using the Sylgard 184 silicone elastomer kit. In addition to the SIPs, non-imprinted polymer (NIP) chips were made. The protocol used was the same except that pure 1 × PBS was used instead of the *E. coli* stock solution. For comparison, SIP receptor chips were also prepared on glass and aluminum chips.

An optical contact angle device (DataPhysics, OCA 25, Filderstadt, Germany) was used to analyze the wetting behavior of these SIPs and NIPs by the sessile drop method. For all measurements, a 5 µL water drop was dispensed at a rate of 1.0 µL/s onto the surface of interest at 18.0 °C room temperature. Two SIP and two NIP surfaces were analyzed, and for each surface, measurements were performed on two spots. All chips were cleaned with SDS and Milli-Q water prior to measurements.

2.7. Optical and AFM observations

To evaluate the SIPs after imprinting and to ensure complete removal of the bacteria from the cavities after template extraction, images of green-fluorescent *E. coli* expressing mEmerald were recorded with a Leica DM750 M microscope equipped with a HD Digital Camera (Leica MC170 HD) and a LED light source (Leica SFL100, excitation at 470 nm ± 20 nm). A Bruker Multimode 8 atomic force microscope (AFM) with MSNL-F cantilevers (f = 110–120 kHz, k = 0.6 N/m, average tip radius of 2–12 nm) was used for topographical imaging in PeakForce Tapping® mode. The AFM topography images were leveled, line-corrected and measured (height profiles) using Gwyddion software (Necas and Klapetek, 2012).

2.8. Dose-response behavior

Dose-response measurements of the R_{th} signal to detect *E. coli* were performed with two different liquids: For the first case with pure PBS as medium, a dilution series of overnight grown *E. coli* bacteria in pure 1 × PBS solution was constructed with OD600 estimated concentrations of 50, 100, 500, $1{\cdot}10^3$, $5{\cdot}10^3$, $1{\cdot}10^4$, $5{\cdot}10^4$ and $2{\cdot}10^5$ CFU/mL. In the second case, the bacteria in 1 × PBS (5 vol.-%) were diluted with 95 vol.-% apple juice, resulting in the effective concentrations 0, 50, 100, 500, $1{\cdot}10^3$, $5{\cdot}10^3$, $1{\cdot}10^4$, $5{\cdot}10^4$, $1{\cdot}10^5$, $2{\cdot}10^5$ and $1{\cdot}10^6$ CFU/mL. In both cases the exposure protocol was identical and the values given for flow rates, injection times and stabilization periods were optimized by a systematic variation of all parameters. The flow cell was filled with 1 × PBS and left to stabilize for 5–10 min. After starting the measurement, the PBS was refreshed after 30 min and then the device was left to stabilize for another hour to define the baseline of the R_{th} signal. Then, the first and lowest cell concentration was measured using a four-step exposure protocol, which is illustrated in Fig. 3A exemplarily for the exposure to $5{\cdot}10^4$ CFU/mL of *E. coli*. Exactly the same protocol was used for each concentration of the dilution series in the order of increasing concentration.

In the first step ("cell injection"), the cell suspension with the given concentration is delivered to the flow cell over a period of 5 min with a flow rate of 0.2 mL/min (1.0 mL in total) using a computer-controlled, automated syringe pump. In the second step ("cell sedimentation"), the flow halts, allowing the bacteria to sediment and bind to the SIP layer for a period of 20 min. In order to remove cells that are not bound specifically to the chip, we performed a third step involving flushing with pure PBS (5 min with 0.2 mL/min flow rate for a total volume of 1.0 mL). In the fourth step ("equilibrating"), the flow is stopped, and the sensor device is again allowed to reach thermal equilibrium for a period of 20 min. During the entire measurement series, the heater temperature (T_1) was kept constant at 37.0 °C, the ambient temperature being stable at 18.0 ± 0.1 °C.

2.9. Cross-sensitivity testing

The SIPs imprinted for *E. coli* were also tested for their response to four closely related bacterial species, resembling *E. coli* in shape, size and cell membrane composition; i.e. *Citrobacter freundii*, *Hafnia alvei*, *Serratia marcescens* and *Escherichia blattae*. Each measurement started in PBS and after 30 min, fresh PBS was injected into the flow cell and left to stabilize for an additional 60 min. Next, a $1{\cdot}10^6$ CFU/mL concentration of a selected bacterial strain was injected. This high concentration was chosen on purpose to allow detecting very low levels of cross-sensitivity. After 25 min, the flow cell was flushed with pure PBS and again left to stabilize for 25 min. All injections were performed at a rate of 0.2 mL/min for 5 min, with a total injected volume of 1 mL. During all measurements, the heater temperature (T_1) was kept constant at 37.0 °C. The same measurement was also done for a $1{\cdot}10^6$ CFU/mL concentration of *E. coli* as a reference. The resulting signals from the five individual measurements were then compared to assess the cross-sensitivity of these competitors with respect to the *E. coli* SIP. Each measurement was performed using a new SIP to ensure identical conditions. All SIPs for this purpose had been produced in the same batch.

3. Results and discussion

3.1. SIP receptor chips

Fig. 2 shows a fluorescence microscope image and selected AFM images of a SIP imprinted with *E. coli*. As a reference, the inset of Fig. 2A shows the scanning electron microscope (SEM) image of an individual *E. coli* bacterium. The average *E. coli* bacterium has a diameter of 0.25–1 µm and a length of about 2 µm. The cavities resulting from the imprinting process match these dimensions perfectly (Fig. 2B). To confirm the cavities were created by the imprinted bacteria, an AFM image was taken before and after the washing step. In order to determine the homogeneity of the surface coverage of the SIP, a fluorescence microscopy image was taken before the washing step, exploiting the fact that fluorescent *E. coli* were used to make the imprints (Fig. 2A). Another fluorescence microscopy image was taken after the washing step to confirm that all fluorescent *E. coli* were removed during washing. To estimate the surface coverage of the SIP receptor chip, a 20 × 20 μm^2 AFM image was taken (Fig. 2C), resulting in a value of 6.5 (± 0.7) $\cdot 10^6$ cavities/cm^2. The SIP technique can be used on various support materials, as shown by the AFM images in Fig. 2D–F.

The average contact angle of the NIP surfaces is 72.0 ± 3.0°, which is comparable to literature values for polyurethane, thus confirming that the surface is covered with a polyurethane layer (Pergal et al., 2013; Yongabi et al., 2018). On the other hand, the average contact angle on the SIP layers is 101.2 ± 2.2°. This increase in contact angle of polyurethane layers imprinted with cells has been reported in previous studies on SIPs synthesized by imprinting yeast cells (Yongabi et al., 2018).

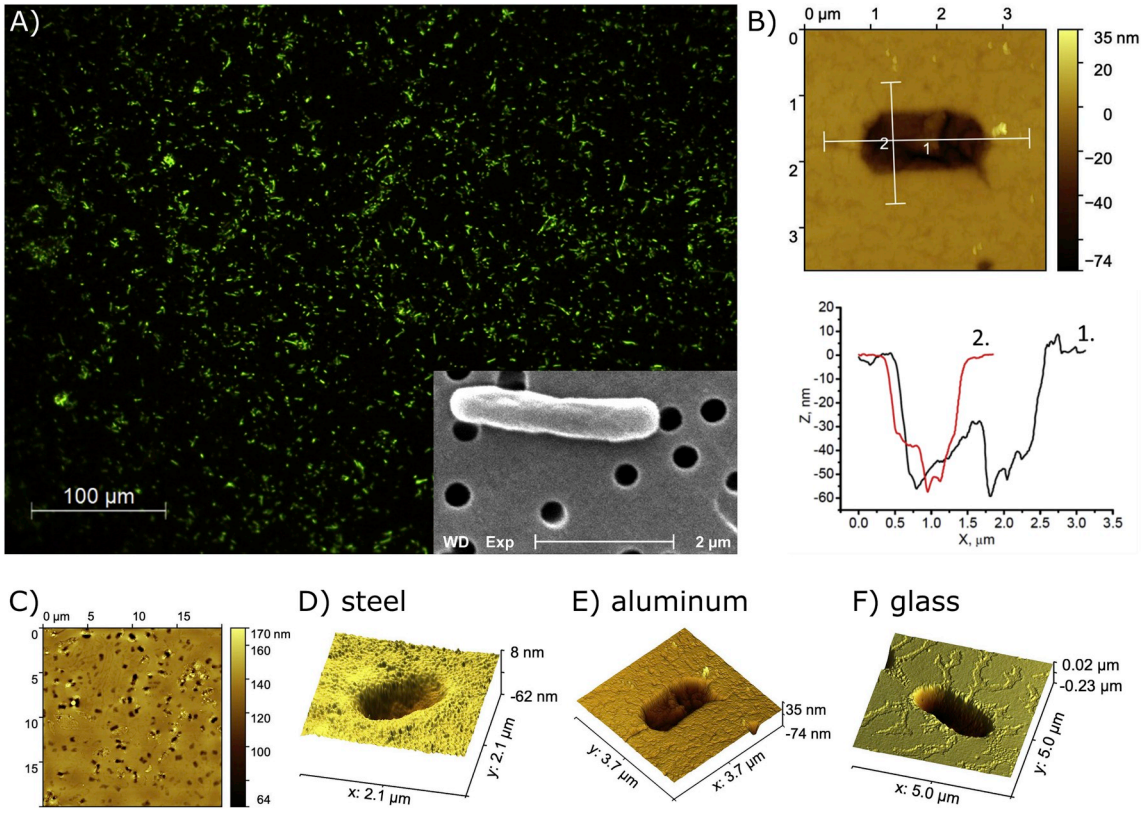

Fig. 2. A) Fluorescence image of a SIP imprinted on steel with fluorescent *E. coli* before the washing (magnification: 20×) (inset: SEM image of a single *E. coli* bacterium at 12800× magnification) B) AFM profile analysis of a cavity created by the imprinting process. Length (1.9 µm) and width (0.96 µm) correspond very well to the size of an *E. coli* bacterium. The depth of the cavity (50 nm) is about one fifth of the thickness of the bacterium, the polyurethane layer is about 1 µm thick. C) AFM overview image used to calculate the surface coverage of the SIP receptor chip. D-F) 3D AFM images of an empty cavity made on different support materials (respectively steel, aluminum and glass).

3.2. Dose-response characterization with PBS medium

Fig. 3B shows the recognition experiment for an *E. coli* SIP which was exposed to increasing *E. coli* concentrations in PBS, starting from pure PBS over 50 CFU/mL to $2{\cdot}10^5$ CFU/mL. The sensor chip was not regenerated between the measurement for a given concentration and the next-higher concentration owing to the difficulty to perform an efficient regeneration protocol inside the limited volume of the flow cell. The R_{th} value displays a systematic, stepwise increase and the apparent spikes in between the different concentrations arise from introducing liquids (cell suspensions and pure PBS) at room temperature into the flow cell. This causes a temporary drop of the T_2 parameter, resulting in sharp maxima of the R_{th} signal. For the highest concentration of $2{\cdot}10^5$ CFU/mL, the total increase in R_{th} with respect to the baseline (established with pure PBS) is 3.6 °C/W. This is twice the difference of $\Delta R_{th} \approx 1.7$ °C/W that was measured for the same concentration of *E. coli* using the classical heat-transfer method with a separate power source and two thermocouples (van Grinsven et al., 2016).

The R_{th} data used to generate the dose-response curves shown in Fig. 3C and D were collected for each of the concentrations in twofold: In the sedimentation step (data collection A, see Fig. 3A) and in the equilibration step (data collection B, see Fig. 3A), for which the data of the final 5 min was taken where the R_{th} signal is stable without variation over time. For each of the two data sets, we calculated the numerical average and the standard deviation σ, which defines the height of the error bars in Fig. 3C and D. The goal of the equilibrating step is to have the flow cell filled with the pure buffer, thereby removing the influence of unbound cells on the R_{th} measurements.

The twofold data set obtained with *E. coli* in pure PBS reveals an interesting observation: The R_{th} values obtained in the equilibrating phase (after rinsing with pure PBS) are systematically higher than the R_{th} values in the cell-sedimentation phase, where a fraction of the administered bacteria is bound to the SIP chip while there are also unbound bacteria in the liquid. This proves directly that PBS containing cells has a lower thermal resistivity (higher thermal conductivity) than pure PBS. The fact that particles in a liquid enhance its thermal conductivity is known in literature from so-called “nanofluids” containing a small volume fraction of metal- or oxide nanoparticles (Eastman et al., 2001; Keblinski et al., 2005). Such additions can enhance the fluids’ thermal conductivity by up to orders of magnitude and our results suggest that the effect is also present when cells are suspended in an electrolyte.

Thanks to this observation, the data point for the lowest concentration (100 CFU/mL) in the rinsed state, see Fig. 3C, lies already above the 3σ interval that defines the experimental uncertainty. Hence, there is a measured detection limit of 100 CFU/mL for the case with PBS buffer as matrix medium. Measurements of the entire concentration series were performed several times, recurrently showing this particularly low detection limit. The concentration axis in Fig. 3C is presented on a logarithmic scale and the dose-response fit function (Yadav, 2013) is based on the following equation (Eq. (2)) incorporated in the Origin™ software package:

$$R_{th} = A_1 + \frac{(A_2 - A_1)}{(1 + 10\hat{}((\log(C_0) - C).\, p))} \quad (2)$$

The goodness factor R^2 of the fit is 0.96 when pure PBS is present above the sensitive area (data collection B) and $R^2 = 0.92$ when the liquid contains unbound *E. coli* cells (data collection A). As can be expected, the difference between both data points becomes more

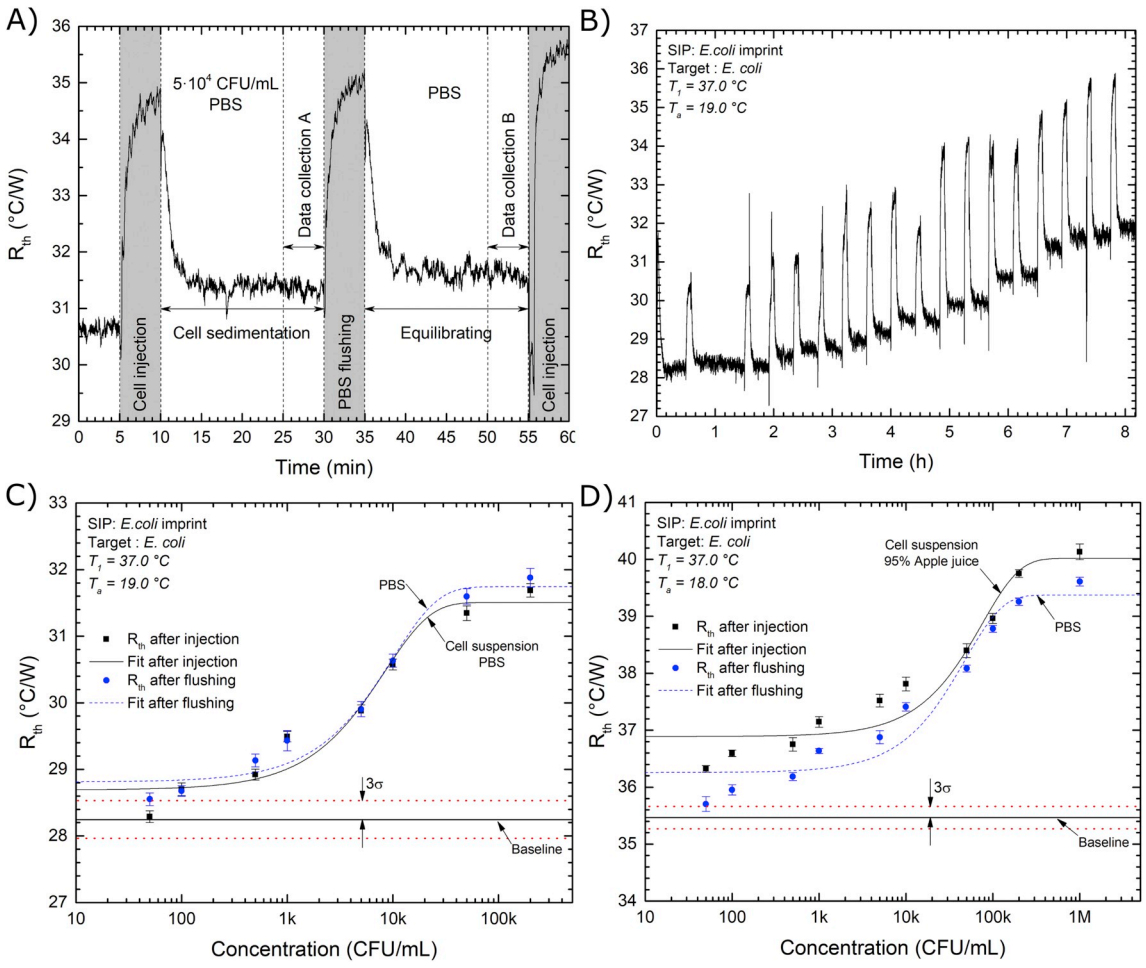

Fig. 3. A) Detailed example of the four-step exposure protocol: The cell suspension injection during 5 min at a rate of 0.2 mL/min is followed by 20 min sedimentation time, 5 min of PBS flushing at 0.2 mL/min, and finally 20 min of equilibration. B) Dose-response experiment performed on a SIP imprinted with *E. coli*. The SIP was exposed to increasing concentrations of target cells in PBS buffer (50, 100, 500, $1{\cdot}10^3$, $5{\cdot}10^3$, $1{\cdot}10^4$, $5{\cdot}10^4$, and $2{\cdot}10^5$ CFU/mL) alternated with PBS flushing. The thermal resistance increases noticeably in a systematic, concentration-dependent manner. C and D) Dose-response curves for respectively *E. coli* in PBS and *E. coli* in 95% apple juice were created based on data sets from collection point A (sedimentation step, black squares) and collection point B (equilibration step, blue circles). Dose-response fits of the obtained data sets yielded R^2-values of respectively 0.92 (dataset A, PBS), 0.96 (dataset B, PBS), 0.90 (dataset A, 95% apple juice), and 0.91 (dataset B, 95% apple juice). The red dotted line corresponds to the 3σ level, defined as three times the standard deviation of the baseline measurement. Error margins were calculated as the standard deviation of the measurement during the 5-min data collection period. (For interpretation of the references to colour in this figure legend, the reader is referred to the Web version of this article.)

pronounced when the concentration increases, the largest difference being observed for $2{\cdot}10^5$ CFU/mL.

3.3. Dose-response in apple juice

The upper legal norm for *E. coli* in unpasteurized fruit juice is 1000 CFU/mL, see Table 1. In contrast to the measurement in a PBS matrix, the twofold data set obtained with *E. coli* in 95% apple juice shows R_{th} values obtained in the equilibrating phase (hence after rinsing with pure PBS) to be systematically lower than the R_{th} values in the cell-sedimentation phase. Therefore, we can conclude that apple juice has a higher thermal resistivity than pure PBS, as confirmed by the higher R_{th} of a 95% apple juice solution without *E. coli* compared to pure PBS. The concentration axis in Fig. 3D is also on a logarithmic scale and the dose-response fit function is based on equation (Eq. (2)). In this case, the goodness factor R^2 of the fit is 0.91 when pure PBS is present (data collection B) and $R^2 = 0.90$ when the liquid contains unbound *E. coli* cells with 95% apple juice as the medium (data collection A). The obtained limit-of-detection is roughly the same as for the measurement in a pure PBS matrix, more specifically 100 CFU/mL. Moreover, the ΔR_{th} of data collection B, for example at $2{\cdot}10^5$ CFU/mL, is very similar, with values of 3.63 °C/W and 3.79 °C/W, respectively for the PBS and apple juice matrix.

3.4. Cross-sensitivity testing with Enterobacteriaceae

For a reliable identification of *E. coli* contaminations, it is important that the sensor system is adequately specific and not susceptible to false-positive results, which may originate from related organisms. It has recently been demonstrated that SIP receptors for *E. coli*, prepared with the same protocol we used here, have an unmeasurably low cross-sensitivity for a wide range of potential competitors including *Staphylococcus aureus*, *Klebsiella pneumonia*, *Pseudomonas aeruginosa*, *Enterococcus cecorum*, *Staphylococcus epidermidis*, *Acinetobacter baumannii*, and *Clostridium difficile* (Steen Redeker et al., 2017). Furthermore, target cells can be selectively detected when they are mixed with a hundredfold excess of competitor cells (van Grinsven et al., 2016). As a persistent limitation, SIP receptors cannot yet distinguish between different *E. coli* strains, but this is less relevant when developing a sensor that should be sensitive to all possible subtypes of *E. coli* in order to assess conformance with legal microbiological criteria (Table 1).

In the present work, we pushed cross-sensitivity experiments a step

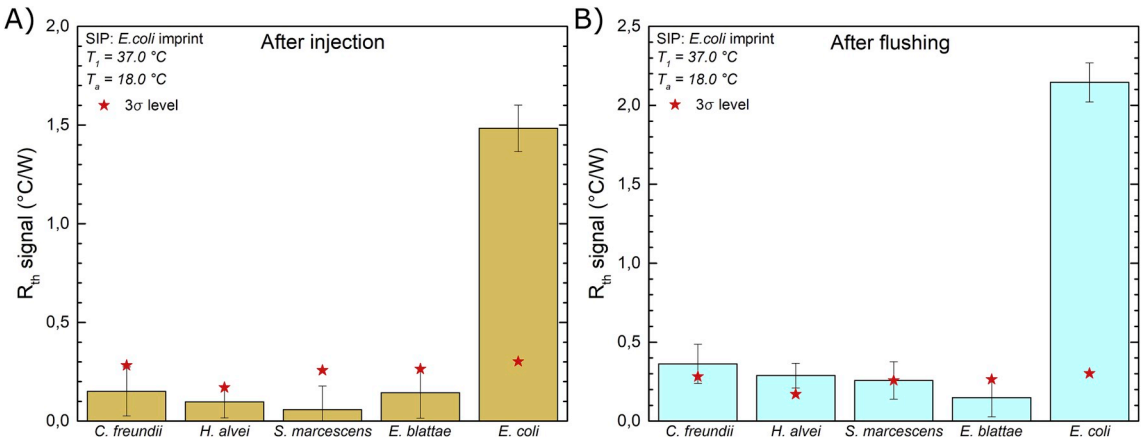

Fig. 4. Cross-sensitivity measurements with four coliform species of the *Enterobacteriaceae* family besides *E. coli*. All concentrations were uniformly $1{\cdot}10^6$ CFU/mL. The red stars represent the 3σ level of each measurement as defined from baseline. Error margins were calculated as the standard deviation of the measurement during the 5-min data collection. A) After injection, with unbound cells still present in the medium, all measurements except the one with *E. coli* are below the detection limit. B) After flushing, without unbound cells in the medium, only two bacteria (*C. freundii* and *H. alvei*), besides *E. coli*, show a response above the detection limit. However, these responses are still more than five times lower when compared to the response obtained for *E. coli*. (For interpretation of the references to colour in this figure legend, the reader is referred to the Web version of this article.)

further by testing the sensor with related *Enterobacteriaceae*. Fig. 4 shows the results of the cross-sensitivity measurements in which *E. coli* SIPs were exposed to *E. coli* itself and four closely related members of the *Enterobacteriaceae* family: *C. freundii*, *H. alvei*, *S. marcescens* and *E. blattae*, all with a $1{\cdot}10^6$ CFU/mL concentration. All these bacteria are Gram-negative with very similar dimensions and other features in common. More specifically, together with *E. coli*, the species belonging to these genera make up the coliforms which is traditionally defined as the group of the *Enterobacteriaceae* with the ability to ferment lactose to acid and gas. Both *E. coli* and coliforms are fecal indicator bacteria because they inhabit the gastrointestinal tract of warm-blooded animals (Mara, 2003). Coliforms are found in the aquatic environment, in soil, and on vegetation and therefore several coliform species can be simultaneously present in the same food, water or agricultural sample.

The response after injection, with unbound cells still present in the medium, is below the detection limit for all, except for *E. coli* itself. After flushing, with no unbound cells present in the medium, the response increases for all 5 species. However, the response for *S. marcescens* and *E. blattae* still remains below the detection limit and for *C. freundii* and *H. alvei* only slightly exceeds the detection limit indicating very limited cross-sensitivity to these species. The response for *E. coli* is slightly lower than expected from the dose-response curve. However, in this test the sensor was not previously exposed to lower concentrations, as was done in the dose-response curve of Fig. 3B. These results extend the established knowledge on cross-sensitivity, as described previously (Steen Redeker et al., 2017), and illustrate the discriminatory power of this biomimetic sensor technique to differentiate between *E. coli* and other *Enterobacteriaceae*. This level of selectivity cannot be explained solely by geometry of the cavities in the SIPs because all bacterial strains used are similar in size and shape. Therefore, additional recognition mechanisms must be present. In fact, there is strong evidence that (bio)chemical recognition, caused by remnants of cell membrane incorporated in the surface of the cavities (Gennaro et al., 2018; Yongabi et al., 2018) and the arrangement of functional groups in the cavities (Ren and Zare, 2012) also play a role in the cell-SIP interaction.

3.5. Comparison with the state of the art

An overview of the detection limits for various transducer/receptor combinations, without claiming to be exhaustive, is given in Table 2. This shows that the performance level of the improved HTM sensor is comparable to the best current techniques for bacterial detection. Moreover, it demonstrates its sensitivity in a real food sample (fruit juice), even without further optimization or sample preparation.

3.6. Thermophysical analysis of the device

The baseline R_{th} value of the sensing device before cell recognition was always found in the limited range between 28 °C/W and 36 °C/W throughout all measurements. The scattering of the results arises from the fact that the constituting elements of the device are clamped mechanically, leading to variations in the thermal contact between the elements. The changes in ΔR_{th} upon binding bacteria are always concentration-dependent in the sense that a given dose of bacteria causes the same, absolute ΔR_{th} change, irrespective of the baseline value. A crosscheck calculation confirms that the baseline values comply with the dimensions of the device and the employed materials:

The temperature difference (T_1 – T_2) measured between the meander and the Pt100 resistor in the top lid is related to a thermal current that passes through the electrically insulating Scotch tape (d_{tape} = 40.0 µm, λ_{tape} = 0.75 W/m.K), the steel chip (d_{steel} = 0.2 mm, λ_{steel} = 16.2 W/m.K), the imprinted PU layer (d_{PU} = 1.0 µm, λ_{PU} = 0.025 W/m.K), and the PBS liquid (d_{PBS} = 1.0 mm, λ_{PBS} = 0.6 W/m.K). The thermal conductivity λ values of water, steel, and polymers were taken from the Engineering Toolbox web reference. The meander measures A = 5 × 5 mm^2 and, as a simplification, we will in the following calculation only consider one-dimensional heat transport that is directed upward (from the meander through the liquid to the Pt100 sensor) and downward through the glass chip at the backside of the meander. The expected R_{th} value in the upward direction is calculated as follows; using thermal resistors in series (Eq. (3)):

$$R_{th}(expected) = \frac{1}{A}\left(\frac{d_{PBS}}{\lambda_{PBS}} + \frac{d_{PU}}{\lambda_{PU}} + \frac{d_{steel}}{\lambda_{steel}} + \frac{d_{tape}}{\lambda_{tape}}\right) = 71°C/W \quad (3)$$

This is about twice the baseline value, but one should note that Eq. (1) assumes that the total heating power passes the solid-liquid interface while in reality a fraction of the power dissipates to the ambient through the backside of the chip and in lateral directions. Using the 1D-approximation, we can calculate the R_{th} value of the backside, in which heat passes through the glass chip (d_{glass} = 1.0 mm, λ_{glass} = 1.05 W/m.K), and the PMMA bottom of the device (d_{PMMA} = 1.0 mm, λ_{PMMA} = 0.2 W/m.K) (Eq. (4)):

$$R_{th}(backside) = \frac{1}{A}\left(\frac{d_{glass}}{\lambda_{glass}} + \frac{d_{PMMA}}{\lambda_{PMMA}}\right) = 238°C/W \quad (4)$$

Table 2
Overview of detection limits of bio- and biomimetic sensors for bacterial detection.

Bacterial species[a]	Transducer principle	Receptor type	LoD	Reference
E. coli	Electromagnetic trap	Antibody	$6.6{\cdot}10^6$ CFU/mL (deionized water)	Li and Kosel (2014)
S. paratyphi	SPR	Microcontact imprinted polymer	$1.4{\cdot}10^6$ CFU/mL (water)	(Perçin et al., 2017)
E. coli	QCM	Microcontact imprinted polymer	$3.72{\cdot}10^5$ CFU/mL (water)	Yilmaz et al. (2015)
D. radiodurans, S. natans, E. coli, B. subtilis, C. parvum	Fluorescence microscopy	Imprinted sol-gel films	10^3–10^4 CFU/mL (PBS)	Cohen et al. (2010)
P. aeruginosa, and *S. marcescens*	Dielectrophoresis	Molecularly imprinted polymers (MIP)	10^3 CFU/mL (water), 10^7 CFU/mL (apple juice)	Tokonami et al. (2013)
E. coli, *D. proteolyticus*, *S. epidermidis*, *S. pneumoniae*	EIS	Cell imprinted polymer (CIP)	10^3 CFU/mL (PBS)	Golabi et al. (2017)
S. aureus	ELISA	Artificial antibodies/SIP	500 CFU/mL	Zhang et al. (2015)
C. jejuni	QCM	Mono- and polyclonal antibodies	150 CFU/mL (PBS)	Masdor et al. (2016)
E. coli	Capacitive	Microcontact imprinted sensor	70 CFU/mL (PBS)	Idil et al. (2017)
E. coli	Potentiometric	Aptamers	4 CFU/mL (PBS)	Zelada-Guillen et al. (2010)
E. coli	HTM	SIP	100 CFU/mL (PBS, apple juice)	This study

[a] *Escherichia coli* (*E. coli*), *Salmonella paratyphi* (*S. paratyphi*), *Deinococcus radiodurans* (*D. radiodurans*), *Sphaerotilus natans* (*S. natans*), *Bacillus subtilis* (*B. subtilis*), *Cryptosporidium parvum* (*C. parvum*), *Pseudomonas aeruginosa* (*P. aeruginosa*), *Serratia marcescens* (*S. marcescens*), *Deinococcus proteolyticus* (*D. proteolyticus*), *Staphylococcus epidermidis* (*S. epidermidis*), *Streptococcus pneumoniae* (*S. pneumoniae*), *Staphylococcus aureus* (*S. aureus*), and *Campylobacter jejuni* (*C. jejuni*).

To calculate the total R_{th} for the upward heat flow through the device, the contribution of the titanium cover ($d_{titanium} = 4.0$ mm, $\lambda_{titanium} = 19.4$ W/m.K) needs to be added to Eq. (3), which results in a value of 79 °C/W. The fractions of power that are transmitted upward and downward are inversely proportional to the R_{th} values in the respective directions: In the given situation with $T_1 = 37.0$ °C and $P_{total} = 192$ mW, this corresponds to an upward heat flow $P_{up} = 144$ mW and a heat flow through the backside $P_{down} = 48$ mW. In other words, the majority, namely 75% of the total heating power, passes the biosensitive interface. With this correction factor, the experimental R_{th} values (between 28 and 36 °C/W) translate into 37–48 °C/W, which agrees reasonably with the expected R_{th} value of 71 °C/W. Using more refined calculations, this model can be extended to three dimensions to include sideways heat dissipation and thermal boundary resistances between dissimilar materials. For the time being, the agreement between the 1D-model and the experimental results is satisfactory.

4. Conclusions

For this work, stainless-steel was selected because of its corrosion resistance, as most biosensor applications require contact with liquids, and its relatively high thermal conductivity, which benefits the HTM principle. It is also a low-cost material, which is another advantage as the SIP receptor chip is the only consumable part of the setup. The bifunctional meander is a fixed part of the device that only needs to be recalibrated periodically. The entire device is not larger than a matchbox and in principle, it is also suitable for in-line applications due to the long-term stability of the synthetic SIP receptors.

The HTM setup, developed in this work, reaches a LoD of 100 CFU/mL, which is at the low end of the currently documented state-of-the-art sensor methods, irrespective of the underlying receptor type and transducer principle. Moreover, this concentration was actually measured and not extrapolated from higher concentrations. Even in the complex matrix of non-cleared apple juice, the LoD stays the same, underpinning the relevance of this new development for food safety analysis.

The SIP receptor chips were subjected to a stringent cross-sensitivity test resulting in a specific signal generated only for *E. coli* and not for the related species, all belonging to the coliform group of the *Enterobacteriaceae* family. These SIP receptors can be synthesized on a wide variety of readily available support materials.

The improved HTM device has now reached a performance level which brings the original HTM concept for cell detection from 2013 (Eersels et al., 2013) very close to real-life applications. Moreover, it is a generic concept which can be easily adapted for other micro-organisms. The proof of concept delivered here for bacterial detection in real life food applications can be used in a broader sense for environmental monitoring, agriculture and the diagnostics of infectious diseases.

Declaration of interests

The authors declare that they have no known competing financial interests or personal relationships that could have appeared to influence the work reported in this paper.

The authors declare the following financial interests/personal relationships which may be considered as potential competing interests:

Conflicts of interests

The authors declare no conflicts of interest.

CRediT authorship contribution statement

Peter Cornelis: Conceptualization, Data curation, Formal analysis, Investigation, Methodology, Software, Validation, Writing - original draft. **Stella Givanoudi:** Investigation, Methodology, Validation, Visualization. **Derick Yongabi:** Investigation, Methodology, Validation, Visualization, Writing - review & editing. **Heiko Iken:** Resources. **Sam Duwé:** Resources, Writing - original draft. **Olivier Deschaume:** Visualization. **Johan Robbens:** Conceptualization, Funding acquisition. **Peter Dedecker:** Funding acquisition, Resources, Writing - original draft. **Carmen Bartic:** Visualization. **Michael Wübbenhorst:** Conceptualization, Funding acquisition, Methodology. **Michael J. Schöning:** Conceptualization, Resources, Writing - original draft. **Marc Heyndrickx:** Conceptualization, Methodology, Supervision, Validation, Writing - original draft. **Patrick Wagner:** Conceptualization, Funding acquisition, Methodology, Project administration, Supervision, Writing - review & editing.

Acknowledgements

Financial support by the Research Foundation Flanders, project #G079116N ("Utilizing interfacial impedance and heat-transfer phenomena in advanced monitoring and switching devices"), and the

postdoctoral fellowship of Sam Duwé, the KU Leuven FLOF scholarship (P. Cornelis), and the KU Leuven C1 project, C14/15/067 “Smart Cellular Scaffolds”, and the ERASMUS travel fellowship of the European Union of I. Thomas, who assisted in creating the AFM images, are gratefully acknowledged. P. Dedecker acknowledges support from the FWO via grant #G0B8817N (“Assessing dimerization-based regulation of GPCRs using live-cell activity and interaction sensing in genomically-labeled neurons”). C. Bartic and O. Deschaume acknowledge support from the FWO via grant #G094717N (“NeuroActive Light-Addressable Nanoparticle-Protein Matrices”), and O. Deschaume also acknowledges the financial support from the KU Leuven C1 project, C14/16/063 “OPTIPROBE”. S. Givanoudi received an ILVO PhD research grant in the frame of ISense. Technical support by W. Neefs (KU Leuven) and cell culturing support by G. Wackers (KU Leuven) are greatly appreciated.

References

Bäcker, M., Pouyeshman, S., Schnitzler, T., Poghossian, A., Wagner, P., Biselli, M., Schöning, M.J., 2011. A silicon-based multi-sensor chip for monitoring of fermentation processes. Phys. Status Solidi 208 (6), 1364–1369.

Betlem, K., Hoksbergen, S., Mansouri, N., Down, M., Losada-Pérez, P., Eersels, K., van Grinsven, B., Cleij, T.J., Kelly, P., Sawtell, D., Zubko, M., Banks, C., Peeters, M., 2018. Real-time analysis of microbial growth by means of the heat-transfer method (HTM) using *Saccharomyces cerevisiae* as model organism. Phys. Med. 6, 1–8.

Chambers, J.P., Arulanandam, B.P., Matta, L.L., Weis, A., Valdes, J.J., 2008. Biosensor recognition elements. Curr. Issues Mol. Biol. 10, 1–12.

Cohen, T., Starosvetsky, J., Cheruti, U., Armon, R., 2010. Whole cell imprinting in sol-gel thin films for bacterial recognition in liquids: macromolecular fingerprinting. Int. J. Mol. Sci. 11 (4), 1236–1252.

Council Directive 98/83/EC of, 3 November 1998. On the Quality of Water Intended for Human Consumption.

Dewaele, I., Ducatelle, R., Herman, L., Heyndrickx, M., De Reu, K., 2011. Sensitivity to disinfection of bacterial indicator organisms for monitoring the *Salmonella enteritidis* status of layer farms after cleaning and disinfection. Poultry Sci. 90 (6), 1185–1190.

Dickert, F.L., Hayden, O., Halikias, K.P., 2001. Synthetic receptors as sensor coatings for molecules and living cells. Analyst 126 (6), 766–771.

Eastman, J.A., Choi, S.U.S., Li, S., Yu, W., Thompson, L.J., 2001. Anomalously increased effective thermal conductivities of ethylene glycol-based nanofluids containing copper nanoparticles. Appl. Phys. Lett. 78 (6), 718–720.

EC, 2003. Proposal for a Directive of the European Parliament and of the Council Concerning the Quality of Bathing Water (2003/C 45 E/15) COM(2002) 581 Final - 2002/0254(COD).

EC, 2007. Commission Regulation (EC) No 1441/2007 of 5 December 2007 Amending Regulation (EC) No 2073/2005 on Microbiological Criteria for Foodstuffs.

Eersels, K., Lieberzeit, P., Wagner, P., 2016. A review on synthetic receptors for bioparticle detection created by surface-imprinting techniques - from principles to applications. ACS Sens. 1 (10), 1171–1187.

Eersels, K., van Grinsven, B., Ethirajan, A., Timmermans, S., Jimenez Monroy, K.L., Bogie, J.F., Punniyakoti, S., Vandenryt, T., Hendriks, J.J., Cleij, T.J., Daemen, M.J., Somers, V., De Ceuninck, W., Wagner, P., 2013. Selective identification of macrophages and cancer cells based on thermal transport through surface-imprinted polymer layers. ACS Appl. Mater. Interfaces 5 (15), 7258–7267.

Gennaro, A., Yongabi, D., Deschaume, O., Bartic, C., Wagner, P., Wübbenhorst, M., 2018. Cell detection by surface imprinted polymers (SIPs) - a study of the sensor surface by optical and dielectric relaxation spectroscopy. IEEE Trans. Dielectr. Electr. Insul. 25 (3), 816–821.

Golabi, M., Kuralay, F., Jager, E.W.H., Beni, V., Turner, A.P.F., 2017. Electrochemical bacterial detection using poly(3-aminophenylboronic acid)-based imprinted polymer. Biosens. Bioelectron. 93, 87–93.

Hayden, O., Mann, K.J., Krassnig, S., Dickert, F.L., 2006. Biomimetic ABO blood-group typing. Angew Chem. Int. Ed. Engl. 45 (16), 2626–2629.

Idil, N., Hedström, M., Denizli, A., Mattiasson, B., 2017. Whole cell based microcontact imprinted capacitive biosensor for the detection of *Escherichia coli*. Biosens. Bioelectron. 87, 807–815.

ISO, 2001. ISO 16649-2:2001(en). Microbiology of food and animal feeding stuffs - Horizontal method for the enumeration of beta-glucuronidase-positive *Escherichia coli* - Part 2: Colony-count technique at 44 degrees C using 5-bromo-4-chloro-3-indolyl β-D-glucuronide.

Keblinski, P., Eastman, J.A., Cahill, D.G., 2005. Nanofluids for thermal transport. Mater. Today 8 (6), 36–44.

Lazcka, O., Del Campo, F.J., Munoz, F.X., 2007. Pathogen detection: a perspective of traditional methods and biosensors. Biosens. Bioelectron. 22 (7), 1205–1217.

Lenz, M., Striedl, U., Fröhler, 2000. SMD Packages. Thermal Resistance, Theory and Practice. Released by Infineon Technologies AG, Munich, Germany.

Li, F.Q., Kosel, J., 2014. An efficient biosensor made of an electromagnetic trap and a magneto-resistive sensor. Biosens. Bioelectron. 59, 145–150.

Losada-Pérez, P., Jiménez-Monroy, K.L., Grinsven, B.v., Leys, J., Janssens, S.D., Peeters, M., Glorieux, C., Thoen, J., Haenen, K., Ceuninck, W.D., Wagner, P., 2014. Phase transitions in lipid vesicles detected by a complementary set of methods heat-transfer measurements, adiabatic scanning calorimetry, and dissipation-mode quartz crystal microbalance. Phys. Status Solidi 211 (6), 1377–1388.

Mara, D., 2003. Faecal indicator organisms. In: Mara, D., Horan, N. (Eds.), Handbook of Water and Wastewater Microbiology. Academic Press, pp. 105–112.

Masdor, N.A., Altintas, Z., Tothill, I.E., 2016. Sensitive detection of *Campylobacter jejuni* using nanoparticles enhanced QCM sensor. Biosens. Bioelectron. 78, 328–336.

Mehrotra, P., 2016. Biosensors and their applications - a review. J. Oral Biol. Craniof. Res. 6 (2), 153–159.

Morales, M.A., Halpern, J.M., 2018. Guide to selecting a biorecognition element for biosensors. Bioconjug. Chem. 29 (10), 3231–3239.

Nakano, T., Kikugawa, G., Ohara, T., 2010. A molecular dynamics study on heat conduction characteristics in DPPC lipid bilayer. J. Chem. Phys. 133 (15) art. no. 154705.

Necas, D., Klapetek, P., 2012. Gwyddion: an open-source software for SPM data analysis. Cent. Eur. J. Phys. 10 (1), 181–188.

Perçin, I., Idil, N., Bakhshpour, M., Yilmaz, E., Mattiasson, B., Denizli, A., 2017. Microcontact imprinted plasmonic nanosensors: powerful tools in the detection of *Salmonella paratyphi*. Sensors 17 (6) art. no. 1375.

Pergal, M.V., Dzunuzovic, J.V., Poreba, R., Micic, D., Stefanov, P., Pezo, L., Spirkova, M., 2013. Surface and thermomechanical characterization of polyurethane networks based on poly(dimethylsiloxane) and hyperbranched polyester. Express Polym. Lett. 7 (10), 806–820.

Persoons, D., Dewulf, J., Smet, A., Herman, L., Heyndrickx, M., Martel, A., Catry, B., Butaye, P., Haesebrouck, F., 2010. Prevalence and persistence of antimicrobial resistance in broiler indicator bacteria. Microb. Drug Resist. 16 (1), 67–74.

Ren, K.N., Banaei, N., Zare, R.N., 2013. Sorting inactivated cells using cell-imprinted polymer thin films. ACS Nano 7 (7), 6031–6036.

Ren, K.N., Zare, R.N., 2012. Chemical recognition in cell-imprinted polymers. ACS Nano 6 (5), 4314–4318.

Schirhagl, R., Hall, E.W., Fuereder, I., Zare, R.N., 2012. Separation of bacteria with imprinted polymeric films. Analyst 137 (6), 1495–1499.

Steen Redeker, E., Eersels, K., Akkermans, O., Royakkers, J., Dyson, S., Nurekeyeva, K., Ferrando, B., Cornelis, P., Peeters, M., Wagner, P., Dilien, H., van Grinsven, B., Cleij, T.J., 2017. Biomimetic bacterial identification platform based on thermal wave transport analysis (TWTA) through surface-imprinted polymers. ACS Infect. Dis. 3 (5), 388–397.

Stilman, W., Jooken, S., Wackers, G., Cornelis, P., Khorshid, M., Yongabi, D., Akkermans, O., Dyson, S., van Grinsven, B., Cleij, T., van Ijzendoorn, L., Wagner, P., Eersels, K., 2017. Optimization and characterization of a flow cell for heat-transfer-based biosensing. Phys. Status Solidi 214 (9).

Tokonami, S., Nakadoi, Y., Takahashi, M., Ikemizu, M., Kadoma, T., Saimatsu, K., Dung, L.Q., Shiigi, H., Nagaoka, T., 2013. Label-free and selective bacteria detection using a film with transferred bacterial configuration. Anal. Chem. 85 (10), 4925–4929.

Van Dorst, B., Mehta, J., Bekaert, K., Rouah-Martin, E., De Coen, W., Dubruel, P., Blust, R., Robbens, J., 2010. Recent advances in recognition elements of food and environmental biosensors: a review. Biosens. Bioelectron. 26 (4), 1178–1194.

van Grinsven, B., Eersels, K., Akkermans, O., Ellermann, S., Kordek, A., Peeters, M., Deschaume, O., Bartic, C., Diliën, H., Steen Redeker, E., Wagner, P., Cleij, T.J., 2016. Label-free detection of *Escherichia coli* based on thermal transport through surface imprinted polymers. ACS Sens. 1 (9), 1140–1147.

van Grinsven, B., Vanden Bon, N., Strauven, H., Grieten, L., Murib, M., Monroy, K.L., Janssens, S.D., Haenen, K., Schöning, M.J., Vermeeren, V., Ameloot, M., Michiels, L., Thoelen, R., De Ceuninck, W., Wagner, P., 2012. Heat-transfer resistance at solid-liquid interfaces: a tool for the detection of single-nucleotide polymorphisms in DNA. ACS Nano 6 (3), 2712–2721.

WHO, 2011. Guidelines for Drinking-Water Quality, fourth ed. World Health Organization, Geneva, Switzerland.

Yadav, S.K., 2013. Dose-response models to understand toxicodynamics for pollutants in ecosystems. Int. J. Environ. Sci. Dev. Monit. 4 (3), 77–80.

Yilmaz, E., Majidi, D., Ozgur, E., Denizli, A., 2015. Whole cell imprinting based *Escherichia coli* sensors: a study for SPR and QCM. Sensor. Actuator. B Chem. 209, 714–721.

Yongabi, D., Khorshid, M., Losada-Perez, P., Eersels, K., Deschaume, O., D'Haen, J., Bartic, C., Hooyberghs, J., Thoelen, R., Wübbenhorst, M., Wagner, P., 2018. Cell detection by surface imprinted polymers SIPs: a study to unravel the recognition mechanisms. Sensor. Actuator. B Chem. 255, 907–917.

Zelada-Guillen, G.A., Bhosale, S.V., Riu, J., Rius, F.X., 2010. Real-time potentiometric detection of bacteria in complex samples. Anal. Chem. 82 (22), 9254–9260.

Zhang, Z.J., Guan, Y.J., Li, M., Zhao, A.D., Ren, J.S., Qu, X.G., 2015. Highly stable and reusable imprinted artificial antibody used for in situ detection and disinfection of pathogens. Chem. Sci. 6 (5), 2822–2826.

Web references

Engineering Toolbox https://www.engineeringtoolbox.com/thermal-conductivity-d_429.html : data, Accessed date: 13 November 2018.

Finetubes http://www.finetubes.de/uploads/attachments/g145_Legierungen_304_und_304L.pdf, Accessed date: 12 February 2019.

Resistor Guide http://www.resistorguide.com/temperature-coefficient-of-resistance/, Accessed date: 10 October 2016.